Geophysical Research Letters

RESEARCH LETTER
10.1029/2019GL082393

Electron Diffusion Regions in Magnetotail Reconnection Under Varying Guide Fields

L.-J. Chen[1], S. Wang[1,2], M. Hesse[3], R. E. Ergun[4], T. Moore[1], B. Giles[1], N. Bessho[1,2], C. Russell[5], J. Burch[6], R. B. Torbert[6,7], K. J. Genestreti[7], W. Paterson[1], C. Pollock[8], B. Lavraud[9], O. Le Contel[10], R. Strangeway[5], Yu V. Khotyaintsev[11], and P.-A. Lindqvist[12]

[1]NASA, Goddard Space Flight Center, Greenbelt, MD, USA, [2]Department of Astronomy, University of Maryland, College Park, MD, USA, [3]Department of Physics and Technology, University of Bergen, Bergen, Norway, [4]Laboratory of Atmospheric and Space Sciences, University of Colorado Boulder, Boulder, CO, USA, [5]Department of Earth, Planetary, and Space Sciences, University of California, Los Angeles, CA, USA, [6]Southwest Research Institute, San Antonio, TX, USA, [7]Space Science Center, University of New Hampshire, Durham, NH, USA, [8]Denali Scientific, Healy, AK, USA, [9]Institut de Recherche en Astrophysique et Planétologie, Université de Toulouse (UPS), CNRS, CNES, Toulouse, France, [10]Laboratoire de Physique des Plasmas (UMR7648), CNRS/Ecole Polytechnique/Sorbonne Université/Univ. Paris-Sud/Observatoire de Paris, Paris, France, [11]Swedish Institute of Space Physics, Uppsala, Sweden, [12]KTH Royal Institute of Technology, Stockholm, Sweden

Key Points:
- Kinetic structures of three electron diffusion regions under finite guide fields show that meandering remains relevant in all three cases
- Cold inflowing electrons are accelerated along the weak guide field yet fail to follow the local magnetic field at the field minimum
- For an intermediate guide field, wave fluctuations strongly influence electron dynamics in the reconnecting current sheet

Supporting Information:
- Supporting Information S1

Correspondence to:
L.-J. Chen,
li-jen.chen@nasa.gov

Citation:
Chen, L.-J., Wang, S., Hesse, M., Ergun, R. E., Moore, T., Giles, B., et al. (2019). Electron diffusion regions in magnetotail reconnection under varying guide fields. *Geophysical Research Letters*, *46*, 6230–6238. https://doi.org/10.1029/2019GL082393

Received 7 FEB 2019
Accepted 4 JUN 2019
Accepted article online 7 JUN 2019
Published online 24 JUN 2019

Abstract Kinetic structures of electron diffusion regions (EDRs) under finite guide fields in magnetotail reconnection are reported. The EDRs with guide fields 0.14–0.5 (in unit of the reconnecting component) are detected by the Magnetospheric Multiscale spacecraft. The key new features include the following: (1) cold inflowing electrons accelerated along the guide field and demagnetized at the magnetic field minimum while remaining a coherent population with a low perpendicular temperature, (2) wave fluctuations generating strong perpendicular electron flows followed by alternating parallel flows inside the reconnecting current sheet under an intermediate guide field, and (3) gyrophase bunched electrons with high parallel speeds leaving the X-line region. The normalized reconnection rates for the three EDRs range from 0.05 to 0.3. The measurements reveal that finite guide fields introduce new mechanisms to break the electron frozen-in condition.

Plain Language Summary Magnetic reconnection plays a crucial role in the dynamics of the terrestrial magnetotail. For reconnection to occur, the plasma must decouple from the magnetic field. The bounce motion of particles in the magnetotail current sheet is regarded as a key to this decoupling for cases when the current sheet has no magnetic field along the direction of the current. This paper reports that while bounce motion remains relevant when a finite magnetic field is present along the current, new mechanisms to decouple electrons from the magnetic field are introduced, and new open questions unfold. The observations are based on measurements from the Magnetospheric Multiscale mission. The mission's unprecedented high cadence electron data make possible the revelation of the new mechanisms. The results reported in this paper expand the frontiers of our knowledge on magnetotail reconnection and have major implications on the fundamental physics of magnetic reconnection in all plasma systems where binary collisions are not effective, including solar, astrophysical, and laboratory plasmas. Rapid dissemination of the results will set the ground for advances in magnetic reconnection research.

1. Introduction

Magnetotail reconnection underlies a critical part of the substorm dynamics at Earth (e.g., Angelopoulos et al., 2008). How the collisionless plasma in the magnetotail breaks the frozen-in condition to enable reconnection is a fundamental question that has received intense attention. For reconnection with zero guide magnetic field along the electric current, electron meandering—bouncing of demagnetized electrons at the field reversals of the current sheet (e.g., Speiser, 1965)—has been recognized to be central to breaking the frozen in condition [see, e.g., the review paper by Hesse et al., 2011]. Particle-in-cell (PIC) simulations (e.g., Bessho et al., 2014; Chen et al., 2011; Hesse et al., 2018; Ishizawa et al., 2004; Ng et al., 2011; Shuster et al., 2015), in particular, predict that meandering dominates the electron dynamics in the X-line region.

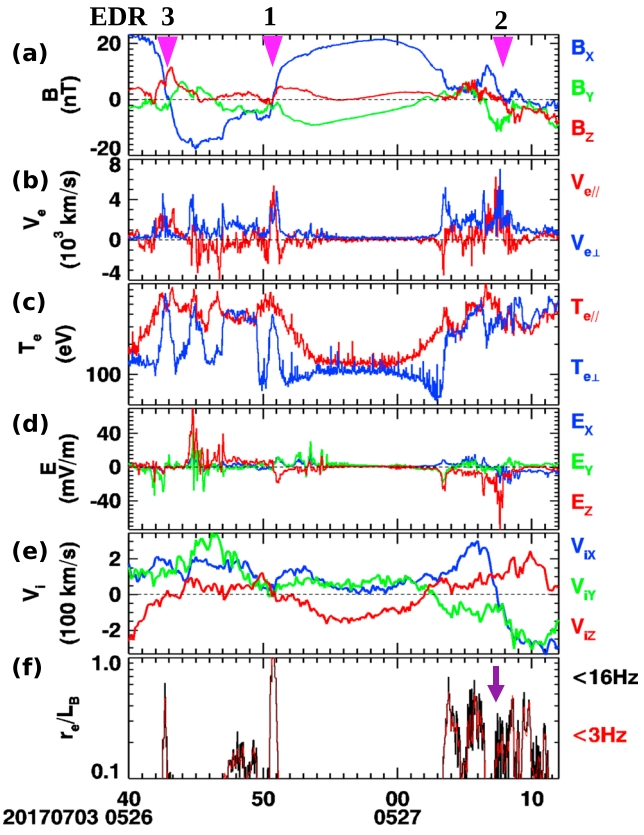

Figure 1. Overview of the electron diffusion regions encountered by Magnetospheric Multiscale 3 in the magnetotail. (a) Three components of the magnetic field ***B***. (b, c) Electron flows and temperatures parallel and perpendicular to ***B***. (d) Electric field components. (e) Ion velocity components. (f) Ratio of the electron thermal gyroradius (r_e) to the magnetic gradient scale ($L_B = |B|/\mu_0|J|$). The black curve plots the ratio r_e/L_B below the Nyquist frequency (16 Hz) of the electron measurements, while the red curve displays r_e/L_B below 3 Hz. The dark violet arrow points to the time when fluctuations above 3 Hz significantly reduce the magnetic gradient scale. All vectors are displayed in Geocentric Solar Magnetospheric unless noted otherwise. EDR = electron diffusion region.

The prediction received vivid confirmation in the measurements of electron distribution functions (DFs) by the Magnetospheric Multiscale (MMS) mission (Burch et al., 2015) showing signatures of electrons bouncing at the field reversal for multiple times and accelerated by the reconnection electric field (Bessho et al., 2017, 2018; Torbert et al., 2018). These signatures are expected to change if the guide field is sufficiently strong to magnetize the electrons throughout the reconnection layer (e.g., Drake et al., 2005; Hesse et al., 2002; Pritchett & Coroniti, 2004). Yet how the signatures vary as the guide field increases remains an outstanding question. This paper reports MMS electron diffusion region (EDR) crossings during magnetotail reconnection under varying guide fields 0.14–0.5 (in unit of the reconnecting component) to address the differing mechanisms to break the frozen-in condition.

The evolution of electron distributions across the EDRs will be emphasized. PIC simulations of symmetric reconnection with finite guide fields (Cattell et al., 2005; Hesse, 2006; Hesse et al., 2004; Ng et al., 2012) predict electron distributions to exhibit field-aligned asymmetry and nongyrotropy in the vicinity of the X-line. How the electron distribution evolves spatially in different parts of the EDR and how the distribution structures reflect the kinetic processes occurring therein are largely unknown. The EDR characteristics reported in this paper expand the frontiers of our knowledge on electron dynamics in magnetotail reconnection.

2. MMS Data

Three EDR crossings will be discussed to address how the electron kinetic features vary with the guide field. All three crossings occur within a 30-s (~10 ion cyclotron periods) interval when MMS threads through the magnetotail current sheet at [−17.6, 3.3, 1.7] R_E in the Geocentric Solar Magnetospheric (GSM) coordinate on 3 July 2017. The reported measurements are all from the MMS3 spacecraft with the Direct Current (DC)- (128 samples per second) from the Flux Gate Magnetometer (Russell et al., 2014) and Alternating Current (AC)-coupled magnetic fields (8,192 samples per second) from the Search-Coil Magnetometer (Le Contel et al., 2016), electric fields (32 samples per second and 8,192 samples per second) from the double probes in the FIELDS suites (Ergun et al., 2014; Lindqvist et al., 2014; Torbert et al., 2014), and electron (30 ms per sample) as well as ion (150 ms per sample) data from the Fast Plasma Investigation (Pollock et al., 2016).

We will employ the local current sheet coordinates labeled as *xyz*, unless otherwise noted. The coordinates *xyz* are defined as follows: *x* is along the outflow (positive toward the Earth), *z* is along the inflow normal to the current sheet, and *y* completes the right-hand orthogonal coordinate (positive in the direction of the reconnection current). Each local current sheet coordinate system is obtained by a hybrid method where *x* is determined from the Minimum Variance Analysis of magnetic fields (Sonnerup & Cahill, 1967), and z is determined using Minimum Faraday Residue (Khrabrov & Sonnerup, 1998) and the timing analysis of magnetic fields (Harvey, 1998). The transformation matrix from GSM to each current sheet coordinate system will be given in the respective figure caption. Considerations and operations specific to each individual current sheet crossing are provided in the supporting information.

3. Results

An overview of the EDR encounters is presented in Figure 1. The EDR intervals to be discussed are around magnetic field B_X reversals (Figure 1a) where intense electron flows (Figure 1b) constitute the main electric current (note that the ***XYZ*** coordinates in Figure 1 are in GSM as the local current sheet coordinates change substantially from one current sheet to the other). The electron temperatures parallel ($T_{e||}$) and

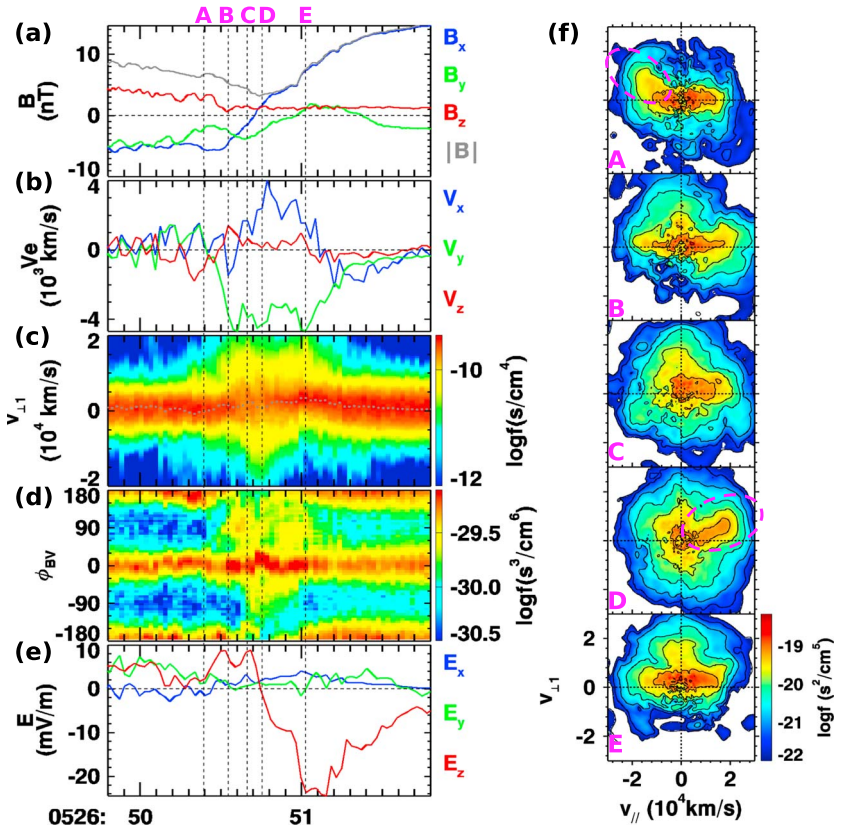

Figure 2. Electron diffusion region 1 with a guide field 0.14. (a) Components of $\boldsymbol{B}$. (b) Components of $\boldsymbol{V_e}$. (c) Electron phase space density as a function of $v_{\perp 1}$ (see text for definition). (d) phase space densities averaged over 3,000–30,000 km/s for each angular bin (defined as ϕ_{Bv}) in the $v_{||}$-$v_{\perp 1}$ plane in the $E \times B$ velocity frame with 0° along $v_{||} > 0$ and 90 toward $v_{\perp 1} > 0$. (e) Electric field components. (f) Electron distribution functions in $v_{||}$-$v_{\perp 1}$ from the time marked by the vertical lines in Figures 2a–2e. All vectors are displayed in the local current sheet coordinates *xyz* unless noted otherwise. The *xyz* unit vectors in Geocentric Solar Magnetospheric ***XYZ*** are (x, y, z) = ([0.9311, −0.2407, 0.2741], [0.0806, 0.8687, 0.4889], [−0.3558, −0.4330, 0.8282]).

perpendicular ($T_{e\perp}$) to the magnetic field display the well documented (e.g., Chen et al., 2008, 2009; Egedal et al., 2010) anisotropy feature of increasing $T_{e||}$and decreasing $T_{e\perp}$ toward the electron current layer inside the ion diffusion region (IDR; Figure 1c), providing the IDR context for the EDRs. The electric field is dominated by the component normal to the nominal tail current sheet, $E_{\boldsymbol{Z}}$ (Figure 1d). $E_{\boldsymbol{Z}}$ is positive below the current sheet ($B_{\boldsymbol{X}} < 0$) and negative above the current sheet ($B_{\boldsymbol{X}} > 0$), consistent with the polarization electric field (also known as the Hall electric field based on the force balance with the Hall term; e.g., Chen et al., 2008) pointing toward the center plane of the electron current layer in the IDR reported in PIC simulations (e.g., Chen et al., 2008; Fujimoto, 2006; Nakamura et al., 2018; Ng et al., 2012), magnetotail observations (e.g., Chen et al., 2008, 2009; Genestreti et al., 2018; Torbert et al., 2018; Wygant et al., 2005), and laboratory measurements (Yamada et al., 2014, 2016; Yoo et al., 2013, 2014).

The EDR identification is based on a combination of active reconnection, proximity to the X-line, and electron demagnetization. Evidence for active reconnection comes in part from ion and electron jets and jet reversals. Correlated with the $B_{\boldsymbol{z}}$ reversal, the ion flow $V_{\boldsymbol{iX}}$ (Figure 1e) reverses at around 052708 UT and is positive or near zero before that, indicating that MMS probes the three EDRs earthward of and in close proximity to the X-line. In all three EDRs to be discussed, the out-of-plane electron flow|V_{ey}| is either larger than or comparable in amplitude with the super-Alfvénic (the upstream Alfvén speed ~900 km/s) electron jet|V_{ex}|(Figures 2–4b), further supporting the proximity to the X-line. Electron demagnetization is indicated by the ratio of the electron thermal gyroradius (r_e) to the magnetic gradient scale L_B (defined as|B|/μ_0|J|, where|J|is taken from the plasma measurements) approaching 1 (Figure 1f, black curve) and the concurrent nongyrotropic electron DFs (Figures 2–4f). Only EDRs involving $B_{\boldsymbol{X}}$ reversals will be discussed in this paper.

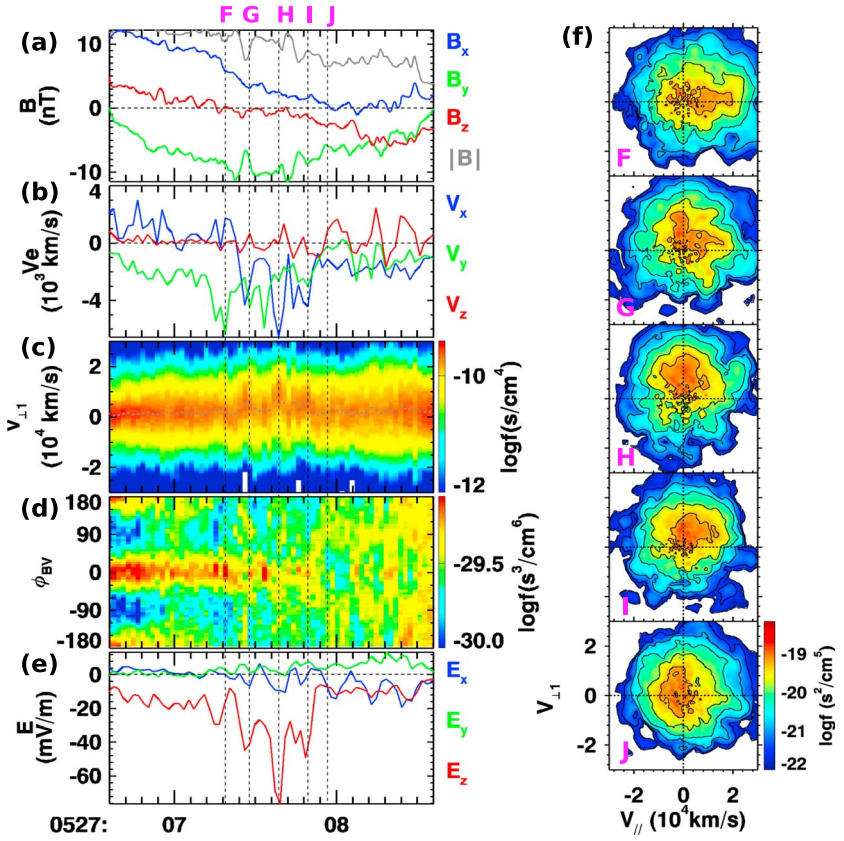

Figure 3. Electron diffusion region 2 with a guide field 0.3. The figure format is the same as that in Figure 2. The *xyz* unit vectors of the local current sheet coordinates in Geocentric Solar Magnetospheric ***XYZ*** are $(x, y, z) = ([0.9910, -0.0513, -0.1240], [0.0331, 0.9889, -0.1445], [0.1300, 0.1391, 0.9817])$.

The density (not shown) in the vicinity of the three EDRs ranges from 0.3 to 0.5 cm^{-3}, yielding an electron skin depth (d_e) 7.5 to 9.5 km.

The three EDRs will be discussed in the order of their guide field strengths, weakest to strongest (numbered 1–3 and marked in Figure 1). EDR 1 has a guide field 0.14, determined based on the B_y (~−3 nT) at the B_x reversal (Figure 2a) and an upstream B_x of 21 nT taken from 052659 UT (Figure 1a). The positive peak of V_{ex} reaches 4,000 km/s within the V_{ey} layer (V_{ey} ~ −4,000 km/s on average within the sharp B_x gradient), and V_{ex} reverses near edges of the layer (Figure 2b), supporting that MMS crosses EDR 1 earthward of the X-line through the super-Alfvénic electron jet where V_{ey} and V_{ex} are comparable.

Detection of accelerated nongyrotropic electrons in the vicinity of the B_x reversal is a major signature of EDRs in the magnetotail (Bessho et al., 2018; Oka et al., 2016; Torbert et al., 2018; Zhou et al., 2019) as well as magnetopause (e.g., Burch et al., 2016; Chen, Hesse, Wang, Bessho, & Daughton, 2016; Chen, Hesse, Wang, Gershman, et al., 2016). To help visualize how nongyrotropy changes over the course of the MMS crossing from outside to inside of the EDR, the reduced DF f as a function of $v_{\perp 1}$ (a velocity unit vector whose direction is defined by $B \times (V_e \times B)$, where B is the averaged magnetic field vector over the sampling time of one electron distribution) and time is plotted in Figure 2c, and Figure 2d displays the phase space densities averaged over 3,000–30,000 km/s (a velocity range where most of the anisotropy and nongyrotropy appear) for each angular bin in the $v_{||}$-$v_{\perp 1}$ plane in the $E \times B$velocity frame with 0° along $v_{||} > 0$ and 90 toward $v_{\perp 1} > 0$. Nongyrotropy is reflected as asymmetry of the phase space density with respect to the core population (with a varying $E \times B$ drift near $v_{\perp 1} = 0$) in Figure 2c and as asymmetry between the phase space density at around +90° and −90° in Figure 2d. Nongyrotropic electrons sandwich the B_x (and E_z) reversal, as indicated by the asymmetries in positive and negative $v_{\perp 1}$ (Figure 2c) and in +90° and −90° of ϕ_{Bv}(Figure 2d), consistent with the enhanced nongyrotropy reported at the boundary of an EDR under a similar level of guide field (Zhou

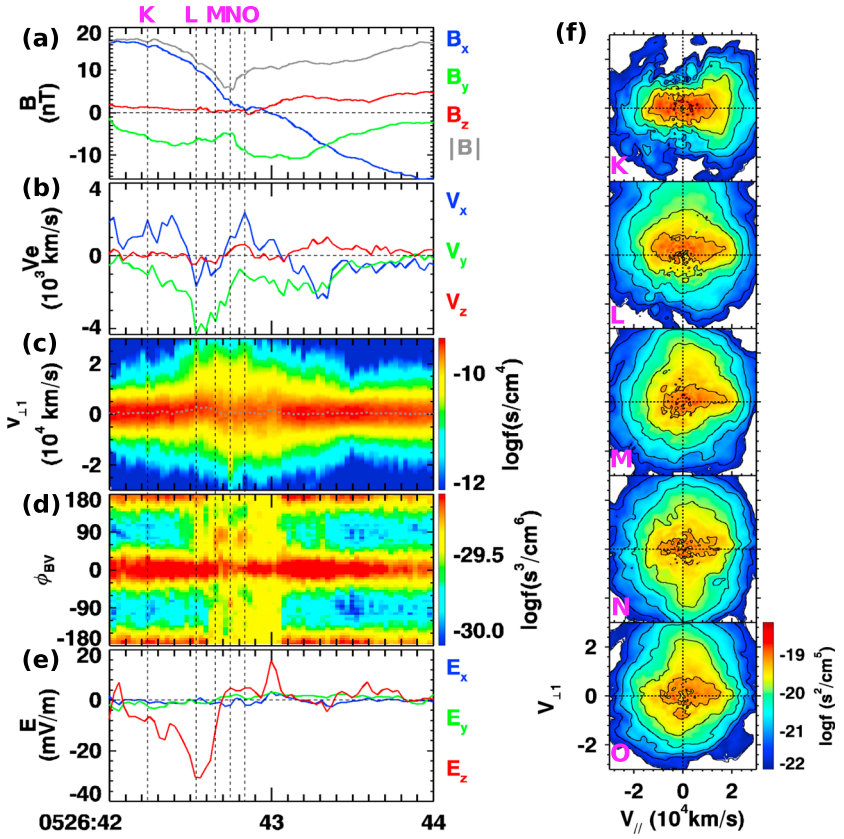

Figure 4. Electron diffusion region 3 with a guide field 0.5. The figure format is the same as that in Figure 2. The *xyz* unit vectors in Geocentric Solar Magnetospheric ***XYZ*** are (*x*, *y*, *z*) = ([0.9840, −0.1685, −0.0578], [−0.0030, 0.3090, −0.9511], [0.1781, 0.9360, 0.3036]).

et al., 2019). This type of nongyrotropy has been recognized to be due to subgyroradius sampling of the EDR-accelerated electrons near the turning points of their meandering orbits (e.g., Chen, Hesse, Wang, Bessho, & Daughton, 2016; Chen, Hesse, Wang, Gershman, et al., 2016).

Features exhibited by EDR 1 are the following: (1) The intense electron flow V_{ey} is due to the $E \times B$ drift of the inflowing population (dotted line in Figure 2c) and the $-y$ ($\sim v_{\perp 1}$) motion of the unmagnetized electrons (shown in the positive high $v_{\perp 1}$ sector of Figure 2c and DFs B, C, and E in Figure 2f). (2) The cold inflowing electrons do not follow the local magnetic field at the|B|minimum (the marked feature in DF D as an example from three consecutive DFs). These electrons are accelerated (can be discerned by the extension to higher $v_{||}$than other DFs) by the reconnection electric field along the direction of the guide field (based on the v_x-v_y distribution—data not shown) yet fail to follow the weak reconnected magnetic field. (3) A new type of nongyrotropy (DF A) is detected right before MMS enters EDR 1. (4) Electrons with $v_{||} < 0$ (away from the X-line) disappear inside the nongyrotropic electron layer (Figure 2d), indicating that crossings of the magnetic separatrices occur within the EDR (e.g., Chen et al., 2017; Chen, Hesse, Wang, Gershman, et al., 2016). (5) The electric field E_z (Figure 2e) is asymmetric about the B_x reversal, likely a result of the finite guide field (e.g., Fu et al., 2018; Ng et al., 2012; Pritchett & Coroniti, 2004). (6) Nongyrotropic electron distributions present a triangular structure in the EDR (e.g., DFs B, C, and E), showing that electrons with lower$|v_{||}|$have higher $v_{\perp 1}$, bearing similarities to those observed with negligible guide field (Torbert et al., 2018). The nongyrotropic electron layer due to finite gyroradius effects (052650.409–052651.249 UT) is estimated to be 113 km ~ 13 d_e.

The new type of nongyrotropy is observed in an electron-scale layer with DF A as one representative example. The defining feature is increasing $v_{\perp 1}$ at higher negative $v_{||}$, (the feature marked with the magenta oval in DF A) indicating that the fastest electrons leaving the X-line region have been accelerated perpendicularly to ***B***. These accelerated electrons are gyrophase bunched, only presenting themselves at positive $v_{\perp 1}$. The

observed velocity dispersion (increasing $v_{\perp 1}$ at increasing $|v_{||}|$) here is opposite to the velocity dispersion (increasing $|v_{\perp}|$ at decreasing $|v_{||}|$) in an asymmetric reconnection exhaust due to the combined time of flight and finite-gyroradius effects of electrons accelerated by parallel electric fields under a guide field of 1 (Hesse et al., 2017). We speculate that the gyrophase bunched electrons are accelerated in the X-line region and have traveled only a fraction of the gyrocycle to get to the observation location along the not-yet-reconnected field lines. If the electrons had traveled more than one gyrocycle, gyrophase mixing would have occurred to smear out the feature of phase bunching. The particle motion in this new type of nongyrotropic distribution differs in nature from that in the crescent distributions due to meandering electrons, and hence, the distribution structure in the velocity plane perpendicular to the magnetic field (not shown) does not take a crescent shape.

The reconnection electric field in EDR 1 is estimated by the measured E_y (effects of the current sheet north-south motion of 135 km/s are removed) averaged over an interval of 0.25 s centered at the B_x reversal, yielding 0.77 ± 0.32 (one standard deviation is provided as the error bar) mV/m, corresponding to 0.05 ± 0.02 if normalized by the upstream $B_0 V_A$. Effects from projection of the finite E_z onto y due to inaccurate coordinate determination should be minimal, as the linear correlation between E_y and E_z discussed by Genestreti et al. (2018) has been removed when determining the coordinate. See supporting information for details about the determination of the coordinates and the current sheet motion.

EDR 2 is encountered when MMS passes through an electron current layer at the correlated reversals of B_z and jets of ions and electrons. The guide field is approximately 30%, deduced by $B_y = -7$ nT at the B_x reversal (Figure 3a). The three largest peaks of$|V_{ex}|$(Figure 3b, approximately marked by the vertical lines G, H, and I) are correlated with E_z (Figure 3e), reflecting that the fastest V_{ex} jet is solely due to the $E_z \times B_y$ drift. In contrast, the fastest V_{ex} jet at $B_x > 0$ locations in EDR 1 is mainly contributed by the projection of a magnetic field-aligned flow onto x.

Of the three reported EDRs, EDR 2 has the highest level of electron flows and fluctuations in the electric and magnetic fields. Two pronounced V_{ey} peaks are observed around the V_{ex} reversal, and they are primarily due to the electron motion parallel to $\boldsymbol{B}$ (Figure 3d and DF F in Figure 3f as an example). The thickness of the nongyrotropic electron layer is estimated to be 30 km (from 052707.359 to 052707.659 UT), using a current sheet z velocity of 100 km/s based on the measured V_{iz} (Figure 1e).

Kinetic structures of EDR 2 are highlighted with snapshots of DFs (DFs F–J). In the current layer near B_z reversal where B_x is weak, nongyrotropic electrons are detected (DF G) and their distributions in the velocity plane perpendicular to B exhibit a crescent structure (not shown), supporting that these electrons are meandering in the current sheet. Within the nongyrotropy layer and the electron jet (V_{ex}<0), wave fluctuations at approximately the lower hybrid frequency (f_{LH}~4–6 Hz) produce bursty electron flows through $E \times B$ and contribute to the fast electron jet. At the peak$|V_{ex}|$and$|E_z|$, electrons are mostly $E \times B$ drifting (DFs G-I and Figure 3c) with a significant degree of nongyrotropy (DF G, for example). Thereafter, the lower-energy population alternates back and forth between positive and negative $v_{||}$as indicated by the distributions (e.g., DFs I-J) and the phase space density concentration alternating between the angular range −90° to 90° and its complement (Figure 3d). The oscillation frequency based on the three clearest cycles (052707.8–052708.5 UT) is again the lower hybrid frequency (~5 Hz).

An initial check to assess whether waves may demagnetize electrons in EDR 2 suggests that the strong wave-driven electron flows could generate electric currents producing magnetic field fluctuations that locally reduce the magnetic gradient scale L_B, leading to a larger r_e/L_B. The fact that the ratio r_e/L_B (black curve in Figure 1f) obtained for frequencies below the Nyquist frequency (16 Hz) of the electron measurements is significantly larger than that using $\boldsymbol{B}$ and $\boldsymbol{J}$ that are low-pass filtered below 3 Hz (red curve) supports this possibility for the interval marked by the dark violet arrow.

The wave fluctuations that strongly influence the electron dynamics during the interval 052707.2–052708.5 UT propagate primarily along $-x$ (perpendicular to the background magnetic field $\boldsymbol{B}$) with a magnetic component along $\boldsymbol{B}$. The electric field fluctuations giving rise to strong $E \times B$ drifts (052707.2–052707.9 UT) have the maximum variance direction 94° from the wave vector $\boldsymbol{k}$ (mainly electromagnetic) and satisfy $k_{\perp}{}^{*}\sqrt{r_e \times r_i} = 0.77$ (where r_e and r_i are the electron and ion thermal gyroradii, respectively), consistent with the long-wavelength lower hybrid wave that typically has $k_{\perp}{}^{*}\sqrt{r_e \times r_i} \sim 1$ (Daughton, 2003). The E fluctuations

modulating electrons along $v_{||}$(052707.9–052708.5 UT) have the maximum variance direction 23° from $\boldsymbol{k}$ (dominantly electrostatic) with $k_{\perp}{}^{*}\, r_e = 0.9$, consistent with the quasi-electrostatic lower hybrid wave that typically satisfies $k_{\perp}{}^{*}\, r_e \sim 1$ (Daughton, 2003)). The wave vectors are determined based on the methods established in Norgren et al. (2012) and Bellan (2016).

The reconnection E field for EDR 2 is estimated from the averaged E_y at B_x reversal (052707.7–052708.1 UT). The value is 4.98 ± 2.27 mV/m, corresponding to 0.31 ± 0.14 in unit of the upstream B_0V_A. The electric field is taken in the spacecraft frame, as the effect of the current sheet motion is expected to be small considering the weak B_x and B_z. For example, having 100-km/s current sheet velocity along z results in a reconnection electric field 5.08 ± 2.28 mV/m and 0.32 ± 0.14 if normalized.

The guide field of EDR 3 is estimated to be 50%, based on $B_y \sim -10$ nT at the nearly simultaneous B_x and B_z reversals (Figure 4a) where the in-plane magnetic field minimum $\sqrt{B_x^2 + B_z^2} \sim 0.38$ nT. The corresponding E_z is 4 mV/m (Figure 4e) and the electron distribution is DF O (Figure 4f). The guide field is strong enough to magnetize the cold inflowing electrons, indicated by the cold electrons primarily aligned with $\boldsymbol{B}$ throughout the shown interval (Figure 4d and DFs K–O).

Despite the cold electrons being magnetized, nongyrotropy is observed in a thin layer. The layer width (up to $B_x = 0$) is estimated to be 57 km ~ 6 d_e, based on nongyrotropic distributions in the interval 052642.429–052642.849 UT with DFs L, M, and O as representative examples. We interpret these DFs as due to meandering electrons performing hybrid orbits of gyration around the guide field and bouncing in the current layer.

At the|B|minimum, nongyrotropy is reduced due to enhancement of electrons with negative $v_{\perp 1}$ and nearly zero $v_{||}$. The existence of these electrons with high negative $v_{\perp 1}$ at weak $v_{||}$could be a result of the strong magnetic curvature exerting forces that redistribute momentum among different pitch angles near the midplane (e.g., Lavraud et al., 2016; Wang et al., 2016). At the edge of the current sheet before entering the nongyrotropic electron layer, electrons with higher positive $v_{||}$(away from the X-line region) exhibit enhanced perpendicular heating (DF K), to be distinguished from the nongyrotropic acceleration shown in DF A. Gyrophase mixing of the electrons that are gyrophase bunched in DF A could result in the perpendicular heating feature in DF K.

The reconnection E field for EDR 3 is estimated from the averaged E_y at the B_x reversal (052642.68–052643.25 UT). After removing the effects of the current sheet velocity (135 km/s along z), the value is 1.62 ± 0.79 mV/m, corresponding to 0.10 ± 0.05 in unit of the upstream B_0V_A.

4. Summary and Conclusion

In summary, kinetic structures of three EDRs in magnetotail reconnection under guide fields 0.14–0.5 are examined. All three EDRs contain a layer of nongyrotropic meandering (used here in a generalized sense to mean a hybrid of gyrating around the guide field and bouncing in the current sheet where the magnetic gradient scale is comparable with the electron gyroradius, as discussed in Chen et al., 2017) electrons, indicating that meandering remains a relevant mechanism to break the frozen-in condition in the reported guide field range.

Under a guide field of 0.14 in EDR 1, a mechanism in addition to meandering to break the frozen-in condition is observed: Cold inflowing electrons field aligned at locations away from the |B| minimum are accelerated along the guide field but fail to follow the local magnetic field at the|B| minimum (DF D in Figure 2). If the guide field is too strong, the electrons are primarily field aligned (such as the case of EDR 3). Without a guide field to channel the cold inflowing electrons, most of the electrons arriving at the EDR|B|minimum would be demagnetized and meander and appear as counterstreaming populations (e.g., Bessho et al., 2018; Chen et al., 2011; Hesse et al., 2018; Ng et al., 2011; Shuster et al., 2015). Gyrophase bunched electrons with high$|v_{||}|$leaving the X-line region are observed on not-yet-reconnected field lines, presenting a new type of nongyrotropy. The interplay between meandering and demagnetized nonmeandering electrons, their respective regimes of operation, and the generation of the gyrophase bunched electrons are among the open questions that require new theory and simulation efforts.

Observations of the three EDRs indicate that finite guide fields may introduce new mechanisms to break the frozen-in condition, depending on the guide field strength. At the ion and electron jet reversals in EDR 2 with a guide field 0.3, large-amplitude wave fluctuations consistent with lower hybrid waves generate bursty electron jets through the $E \times B$ drift and alternate the electron flows between parallel and antiparallel inside the current sheet. Whether and how the waves may demagnetize electrons cause anomalous resistivity and how the waves are excited are questions that remain to be investigated. Under a guide field of 0.5 in EDR 3, nongyrotropy is evident for the higher-energy meandering electrons while the lower-energy electrons remain magnetized throughout the layer.

The estimated reconnection electric fields for the three EDRs range from 0.8 to 5 mV/m, corresponding to 0.05 to 0.3 in normalized units. No consistent trend showing that the reconnection rate increases or decreases with the guide field is discerned.

Acknowledgments
The work was supported by NSF grants AGS-1619584 and AGS-1552142, DOE grant DESC0016278, NASA grants 80NSSC18K1369 and 80NSSC17K0012, and the NASA MMS mission. The French involvement (SCM) on MMS is supported by CNES and CNRS. MMS data are available at the MMS Science Data Center (https://lasp.colorado.edu/mms/sdc/public/).

References

Angelopoulos, V., McFadden, J. P., Larson, D., Carlson, C. W., Mende, S. B., Frey, H., et al. (2008). Tail reconnection triggering substorm onset. *Science*, *321*(5891), 931–935. https://doi.org/10.1126/science.1160495

Bellan, P. M. (2016). Revised single-spacecraft method for determining wave vector k and resolving space-time ambiguity. *Journal of Geophysical Research: Space Physics*, *121*, 8589–8599. https://doi.org/10.1002/2016JA022827

Bessho, N., Chen, L.-J., Hesse, M., & Wang, S. (2017). The effect of reconnection electric field on crescent and U-shaped distribution functions in asymmetric reconnection with no guide field. *Physics of Plasmas*, *24*(7), 072903. https://doi.org/10.1063/1.4989737

Bessho, N., Chen, L.-J., Shuster, J. R., & Wang, S. (2014). Electron distribution functions in the electron diffusion region of magnetic reconnection: Physics behind the fine structures. *Geophysical Research Letters*, *41*, 8688–8695. https://doi.org/10.1002/2014GL062034

Bessho, N., Chen, L.-J., Wang, S., & Hesse, M. (2018). Effect of the reconnection electric field on electron distribution functions in the diffusion region of magnetotail reconnection. *Geophysical Research Letters*, *45*, 12,142–12,152. https://doi.org/10.1029/2018GL081216

Burch, J. L., Moore, T. E., Torbert, R. B., & Giles, B. L. (2015). Magnetospheric multiscale overview and science objectives. *Space Science Reviews*, *199*(1-4), 5–21.

Burch, J. L., Torbert, R. B., Phan, T. D., Chen, L. J., Moore, T. E., Ergun, R. E., et al. (2016). Electron-scale measurements of magnetic reconnection in space. *Science*, *12*(6920), aaf2939. https://doi.org/10.1126/science.aaf2939

Cattell, C., Dombeck, J., Wygant, J., Drake, J. F., Swisdak, M., Goldstein, M. L., et al. (2005). Cluster observations of electron holes in association with magnetotail reconnection and comparison to simulations. *Journal of Geophysical Research*, *110*, A01211. https://doi.org/10.1029/2004JA010519

Chen, L.-J., Bessho, N., Lefebvre, B., Vaith, H., Asnes, A., Santolik, O., et al. (2009). Multi-spacecraft observations of the electron current sheet, neighboring magnetic islands, and electron acceleration during magnetotail reconnection. *Physics of Plasmas*, *16*(5), 56501. https://doi.org/10.1063/1.3112744

Chen, L.-J., Bessho, N., Lefebvre, B., Vaith, H., Fazakerley, A., Bhattacharjee, A., et al. (2008). Evidence of an extended electron current sheet and its neighboring magnetic island during magnetotail reconnection. *Journal of Geophysical Research*, *113*, A12213. https://doi.org/10.1029/2008JA013385

Chen, L.-J., Daughton, W. S., Lefebvre, B., & Torbert, R. B. (2011). The inversion layer of electric fields and electron phase space-hole structure during two-dimensional collisionless magnetic reconnection. *Physics of Plasmas*, *18*(1), 012904. https://doi.org/10.1063/1.3529365

Chen, L.-J., Hesse, M., Wang, S., Bessho, N., & Daughton, W. (2016). Electron energization and structure of the diffusion region during asymmetric reconnection. *Geophysical Research Letters*, *43*, 2405–2412. https://doi.org/10.1002/2016GL068243

Chen, L.-J., Hesse, M., Wang, S., Gershman, D., Ergun, R., Pollock, C., et al. (2016). Electron energization and mixing observed by MMS in the vicinity of an electron diffusion region during magnetopause reconnection. *Geophysical Research Letters*, *43*, 6036–6043. https://doi.org/10.1002/2016GL069215

Chen, L.-J., Hesse, M., Wang, S., Gershman, D., Ergun, R. E., Burch, J., et al. (2017). Electron diffusion region during magnetopause reconnection with an intermediate guide field: Magnetospheric multiscale observations. *Journal of Geophysical Research: Space Physics*, *122*, 5235–5246. https://doi.org/10.1002/2017JA024004

Daughton, W. (2003). Electromagnetic properties of the lower-hybrid drift instability in a thin current sheet. *Physics of Plasmas*, *10*, 3103–3119. https://doi.org/10.1063/1.1594724

Drake, J. F., Shay, M. A., Thongthai, W., & Swisdak, M. (2005). Production of energetic electrons during magnetic reconnection. *Physical Review Letters*, *94*(9), 095001. https://doi.org/10.1103/PhysRevLett.94.095001

Egedal, J., Lê, A., Katz, N., Chen, L.-J., Lefebvre, B., Daughton, W., & Fazakerley, A. (2010). Cluster observations of bidirectional beams caused by electron trapping during antiparallel reconnection. *Journal of Geophysical Research*, *115*, A03214. https://doi.org/10.1029/2009JA014650

Ergun, R. E., Tucker, S., Westfall, J., Goodrich, K. A., Malaspina, D. M., Summers, D., et al. (2014). The axial double probe and fields signal processing for the MMS mission. *Space Science Reviews*, *199*(1-4), 167–188.

Fu, S., Huang, S., Zhou, M., Ni, B., & Deng, X. (2018). Tripolar electric field structure in guide field magnetic reconnection. *Annales Geophysicae*, *36*(2), 373–379. https://doi.org/10.5194/angeo-36-373-2018

Fujimoto, K. (2006). Time evolution of the electron diffusion region and the reconnection rate in fully kinetic and large system. *Physics of Plasmas*, *13*(7), 072904. https://doi.org/10.1063/1.2220534

Genestreti, K. J., Nakamura, T. K. M., Nakamura, R., Denton, R. E., Torbert, R. B., Burch, J. L., et al. (2018). How accurately can we measure the reconnection rate E_M for the MMS diffusion region event of 11 July 2017? *Journal of Geophysical Research: Space Physics*, *123*, 9130–9149. https://doi.org/10.1029/2018JA025711

Harvey, C. C. (1998). In G. Paschmann & P. W. Daly (Eds.), *Spatial gradients and the volumetric tensor, ISSI Sci. Rep. SR-001* (pp. 307–322). Noordwijk, Netherlands: ISSI/ESA.

Hesse, M. (2006). Dissipation in magnetic reconnection with a guide magnetic field. *Physics of Plasmas*, *13*(12), 122107. https://doi.org/10.1063/1.2403784

Hesse, M., Chen, L.-J., Liu, Y.-H., Bessho, N., & Burch, J. L. (2017). Population mixing in asymmetric magnetic reconnection with a guide field. *Physical Review Letters*, *118*(14), 145101. https://doi.org/10.1103/PhysRevLett.118.145101

Hesse, M., Kuznetsova, M., & Birn, J. (2004). The role of electron heat flux in guide-field magnetic reconnection. *Physics of Plasmas*, *11*(12), 5387–5397. https://doi.org/10.1063/1.1795991

Hesse, M., Kuznetsova, M., & Hoshino, M. (2002). The structure of the dissipation region for component reconnection: Particle simulations. *Geophysical Research Letters*, *29*(12), 1563. https://doi.org/10.1029/2001GL014714

Hesse, M., Liu, Y.-H., Chen, L.-J., Bessho, N., Wang, S., Burch, J. L., et al. (2018). The physical foundation of the reconnection electric field. *Physics of Plasmas*, *25*(3), 032901. https://doi.org/10.1063/1.5021461

Hesse, M., Neukirch, T., Schindler, K., Kuznetsova, M., & Zenitani, S. (2011). The diffusion region in collisionless magnetic reconnection. *Space Science Reviews*, *160*(1-4), 3–23. https://doi.org/10.1007/s11214-010-9740-1

Ishizawa, A., Horiuchi, R., & Ohtani, M. (2004). Two-scale structure of the current layer controlled by meandering motion during steady-state collisionless driven reconnection. *Physics of Plasmas*, *11*(7), 3579–3585. https://doi.org/10.1063/1.1758718

Khrabrov, A. V., & Sonnerup, B. U. Ö. (1998). Orientation and motion of current layers: Minimization of the Faraday residue. *Geophysical Research Letters*, *25*(13), 2373–2376. https://doi.org/10.1029/98GL51784

Lavraud, B., Zhang, Y. C., Vernisse, Y., Gershman, D. J., Dorelli, J., Cassak, P. A., et al. (2016). Currents and associated electron scattering and bouncing near the diffusion region at Earth's magnetopause. *Geophysical Research Letters*, *43*, 3042–3050. https://doi.org/10.1002/2016GL068359

Le Contel, O., Leroy, P., Roux, A., Coillot, C., Alison, D., Bouabdellah, A., et al. (2016). The search-coil magnetometer for MMS. *Space Science Reviews*, *199*(1-4), 257–282. https://doi.org/10.1007/s11214-014-0096-9

Lindqvist, P.-A., Olsson, G., Torbert, R. B., King, B., Granoff, M., Rau, D., et al. (2014). The spin-plane double probe electric field instrument for MMS. *Space Science Reviews*, *199*(1-4), 137–165.

Nakamura, T. K. M., Genestreti, K. J., Liu, Y.-H., Nakamura, R., Teh, W.-L., Hasegawa, H., et al. (2018). Measurement of the magnetic reconnection rate in the Earth's magnetotail. *Journal of Geophysical Research: Space Physics*, *123*, 9150–9168. https://doi.org/10.1029/2018JA025713

Ng, J., Egedal, J., Le, A., & Daughton, W. (2012). Phase space structure of the electron diffusion region in reconnection with weak guide fields. *Physics of Plasmas*, *19*(11), 112108. https://doi.org/10.1063/1.4766895

Ng, J., Egedal, J., Le, A., Daughton, W., & Chen, L.-J. (2011). Kinetic structure of the electron diffusion region in antiparallel magnetic reconnection. *Physical Review Letters*, *106*(6), 65002. https://doi.org/10.1103/PhysRevLett.106.065002

Norgren, C., Vaivads, A., Khotyaintsev, Y. V., & André, M. (2012). Lower hybrid drift waves: Space observations. *Physical Review Letters*, *109*(5), 55001. https://doi.org/10.1103/PhysRevLett.109.055001

Oka, M., Phan, T.-D., Oieroset, M., & Angelopoulos, V. (2016). In situ evidence of electron energization in the electron diffusion region of magnetotail reconnection. *Journal of Geophysical Research: Space Physics*, *121*, 1955–1968. https://doi.org/10.1002/2015JA022040

Pollock, C., Moore, T., Jacques, A., Burch, J., Gliese, U., Saito, Y., et al. (2016). Fast plasma investigation for magnetospheric multiscale. *Space Science Reviews*, *199*(1-4), 331–406. https://doi.org/10.1007/s11214-016-0245-4

Pritchett, P. L., & Coroniti, F. V. (2004). Three-dimensional collisionless magnetic reconnection in the presence of a guide field. *Journal of Geophysical Research*, *109*, A01220. https://doi.org/10.1029/2003JA009999

Russell, C. T., Anderson, B. J., Baumjohann, W., Bromund, K. R., Dearborn, D., Fischer, D., et al. (2014). The Magnetospheric Multiscale Magnetometers. *Space Science Reviews*, *199*(1-4), 189–256.

Shuster, J. R., Chen, L.-J., Hesse, M., Argall, M. R., Daughton, W., Torbert, R. B., & Bessho, N. (2015). Spatiotemporal evolution of electron characteristics in the electron diffusion region of magnetic reconnection: Implications for acceleration and heating. *Geophysical Research Letters*, *42*, 2586–2593. https://doi.org/10.1002/2015GL063601

Sonnerup, B. U. O., & Cahill, L. J. Jr. (1967). Magnetopause structure and attitude from Explorer 12 observations. *Journal of Geophysical Research*, *72*(1), 171. https://doi.org/10.1029/JZ072i001p00171

Speiser, T. W. (1965). Particle trajectories in model current sheets: 1. Analytical solutions. *Journal of Geophysical Research*, *70*(17), 4219–4226. https://doi.org/10.1029/JZ070i017p04219

Torbert, R. B., Burch, J. L., Phan, T. D., Hesse, M., Argall, M. R., Shuster, J., et al. (2018). Electron-scale dynamics of the diffusion region during symmetric magnetic reconnection in space. *Science*, *362*(6421), 1391–1395. https://doi.org/10.1126/science.aat2998

Torbert, R. B., Russell, C. T., Magnes, W., Ergun, R. E., Lindqvist, P.-A., LeContel, O., et al. (2014). The FIELDS instrument suite on MMS: Scientific objectives, measurements, and data products. *Space Science Reviews*, *199*(1-4), 105–135.

Wang, S., Chen, L.-J., Bessho, N., Kistler, L. M., Shuster, J. R., & Guo, R. (2016). Electron heating in the exhaust of magnetic reconnection with negligible guide field. *Journal of Geophysical Research: Space Physics*, *121*, 2104–2130. https://doi.org/10.1002/2015JA021892

Wygant, J. R., Cattell, C. A., Lysak, R., Song, Y., Dombeck, J., McFadden, J., et al. (2005). Cluster observations of an intense normal component of the electric field at a thin reconnecting current sheet in the tail and its role in the shock-like acceleration of the ion fluid into the separatrix region. *Journal of Geophysical Research*, *110*, A09206. https://doi.org/10.1029/2004JA010708

Yamada, M., Yoo, J., Jara-Almonte, J., Ji, H., Kulsrud, R. M., & Myers, C. E. (2014). Conversion of magnetic energy in the magnetic reconnection layer of a laboratory plasma. *Nature Communications*, *5*, 4474. https://doi.org/10.1038/ncomms5774

Yamada, M., Yoo, J., & Myers, C. E. (2016). Understanding the dynamics and energetics of magnetic reconnection in a laboratory plasma: Review of recent progress on selected fronts. *Physics of Plasmas*, *23*(5), 055402. https://doi.org/10.1063/1.4948721

Yoo, J., Yamada, M., Ji, H., Jara-Almonte, J., & Myers, C. E. (2014). Bulk ion acceleration and particle heating during magnetic reconnection in a laboratory plasma. *Physics of Plasmas*, *21*(5), 55706. https://doi.org/10.1063/1.4874331

Yoo, J., Yamada, M., Ji, H., & Myers, C. E. (2013). Observation of ion acceleration and heating during collisionless magnetic reconnection in a laboratory plasma. *Physical Review Letters*, *110*(21), 215007. https://doi.org/10.1103/PhysRevLett.110.215007

Zhou, M., Deng, X. H., Zhong, Z. H., Pang, Y., Tang, R. X., el-Alaoui, M., et al. (2019). Observations of an electron diffusion region in symmetric reconnection with weak guide field. *The Astrophysical Journal*, *870*(1), 01. https://doi.org/10.3847/1538-4357/aaf16f